JOURNAL OF GEOPHYSICAL RESEARCH, VOL. 112, C03S21, doi:10.1029/2006JC003523, 2007

Tidal currents in the northwestern Adriatic: High-frequency radio observations and numerical model predictions

C. Chavanne,[1] I. Janeković,[2] P. Flament,[1] P.-M. Poulain,[3] M. Kuzmić,[3] and K.-W. Gurgel[4]

Received 6 February 2006; revised 6 November 2006; accepted 26 December 2006; published 27 March 2007.

[1] A 2-year deployment of high-frequency radio current meters along the Italian coast of the northwestern Adriatic is used to characterize the surface tidal currents. In the middle of the basin, the M_2 and K_1 currents oscillate along the basin axis, but become more circular toward the Italian coast. Comparisons with a 3-D finite-element nonlinear numerical model of the tides show a good agreement for phases in the middle of the basin, although modeled currents amplitudes are overestimated. However, modeled phases lag observed phases by up to 50° (1.7 hours) for M_2 and 100° (6.7 hours) for K_1, and modeled amplitudes are underestimated, in a 10–20 km wide strip along the Italian coast. This shallow (< 30 m deep) region is stratified by low-salinity surface water from the Po, and laterally sheared by the Western Adriatic Current, both absent from the model but possibly affecting tidal propagation. The model may also incompletely parameterize the combined effects of bottom friction and vertical mixing of momentum.

Citation: Chavanne, C., I. Janeković, P. Flament, P.-M. Poulain, M. Kuzmić, and K.-W. Gurgel (2007), Tidal currents in the northwestern Adriatic: High-frequency radio observations and numerical model predictions, *J. Geophys. Res.*, *112*, C03S21, doi:10.1029/2006JC003523.

1. Introduction

[2] The Adriatic tides have been interpreted as co-oscillations with the Ionian and Mediterranean seas, forced through the straight of Otranto [*Defant*, 1914; *Cushman-Roisin and Naimie*, 2002; *Janeković and Kuzmić*, 2005] (see *Cushman-Roisin et al.* [2001] for a review). The semidiurnal tide consists of two oppositely traveling Kelvin waves, one incoming from the Ionian Sea along the eastern coast, the other traveling back along the western coast after reflection at the northern end of the Adriatic. Their superposition results in an amphidrome centered on the basin axis [*Taylor*, 1921]. The diurnal tide is attributed to a topographic wave propagating across the Adriatic Sea [*Malačič et al.*, 2000]. The four major semidiurnal (M_2, S_2, N_2, K_2) and the three major diurnal (K_1, O_1, P_1) constituents exhibit similar intra-group behavior, patterned after the M_2 and K_1 responses [*Janeković and Kuzmić*, 2005].

[3] While the observed tidal elevation patterns are well explained theoretically, relatively little is known about tidal currents due to scarcity of observations. They are weak, less than 15 cm/s, compared to baroclinic and wind-driven currents reaching 50 cm/s [*Orlić et al.*, 1992; *Poulain*, 2001; *Ursella et al.*, 2006]. Separating them is difficult, especially for short time series typical of shipboard ADCP and moored current meter observations.

[4] From year-long repeated ADCP surveys, *Ursella and Gačić* [2001] confirmed the interpretation of the M_2 pattern as a superposition of Kelvin waves, and the K_1 pattern as resulting from a topographic wave. Their vertically-averaged tidal patterns differ between winter and summer, suggesting that baroclinic tides were not entirely removed by vertical averaging. *Cushman-Roisin and Naimie* [2002] found good qualitative agreement between these observations and their 3-D finite element model.

[5] Moored current meters deployed in the northern Adriatic between 44°N and 45°N by *Michelato* [1983] have been used to benchmark several models. *Cavallini* [1985], using a spectral model, reported good agreement for the orientation of the M_2 ellipses, but overestimated their major axis amplitude by 2.3 cm/s on average. *Mosetti* [1986], using a semianalytical model, also found good agreement, consistent with the Kelvin wave description of M_2. *Cushman-Roisin and Naimie* [2002] were able to reproduce both amplitudes and orientations, except at two shallow stations.

[6] Finally, *Janeković and Kuzmić* [2005] validated the predictions of their 3-D finite element model with current meter observations at 9 locations in the northeastern Adriatic. There was good agreement for the semidiurnal currents, but the diurnal currents were generally overestimated.

[1] Department of Oceanography, School of Ocean and Earth Science and Technology, University of Hawaii, Honolulu, Hawaii, USA.
[2] Center for Marine and Environmental Research, Rudjer Bošković Institute, Zagreb, Croatia.
[3] Istituto Nazionale di Oceanografia e di Geofisica Sperimentale, Trieste, Italy.
[4] Institute of Oceanography, University of Hamburg, Hamburg, Germany.

0148-0227/07/2006JC003523$09.00

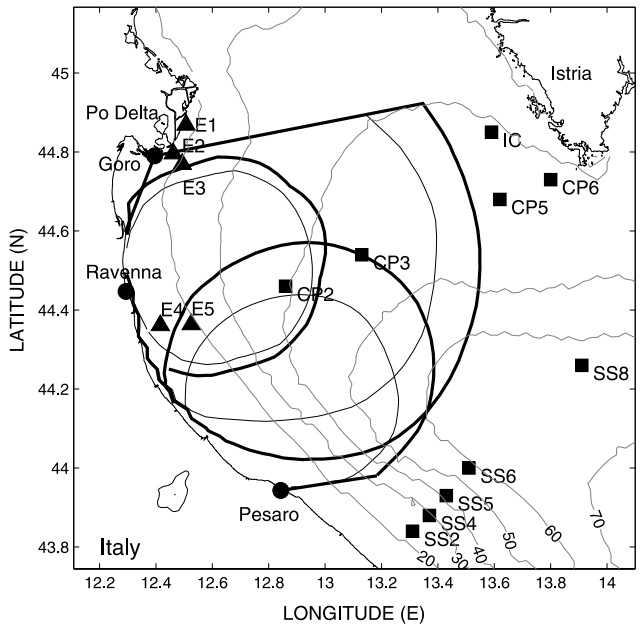

Figure 1. Bathymetry of the northwestern Adriatic (gray lines, in m) and the limits of 50% data coverage, thick lines for nighttime (10pm to 5am UTC) and thin lines for daytime (6am to 9pm UTC). The maximum nighttime/daytime ranges are 102/90 km for Goro, 69/54 km for Pesaro, and 58/52 km for Ravenna. The locations of the HFR's (circles), EuroSTRATAFORM (triangles) and ACE (squares) moorings are indicated.

[7] We present here the harmonic analysis of 2-year time series of currents from high frequency radio (HFR) current meters deployed along the Italian coast between the Po delta and Pesaro. The observed surface tidal currents are compared with the numerical model of *Janeković and Kuzmić* [2005]. The experimental setting and numerical model are described in sections 2 and 3, respectively. Tidal currents are described and compared in section 4, followed in section 5 by a brief description of low-frequency currents to provide the mesoscale context for tidal propagation. The differences between model predictions and observations are discussed in section 6 and summarized in the conclusion. The data processing techniques are described in the appendices.

2. Experimental Setting

[8] Three HFR's were deployed from October 2002 to October 2004 along the Italian coast of the northwestern Adriatic, south of the Po delta (Figure 1), to monitor the surface circulation during the multi-investigator DOLCE-VITA experiment (Dynamics of Localized Currents and Eddy Variability in the Adriatic [*Lee et al.*, 2005]). The FMCW (frequency-modulated continuous-wave) Doppler radios were operated at 16 MHz with 100 kHz chirp width, yielding a range resolution of 1.5 km [*Gurgel et al.*, 1999]. A chirp length of 0.34 s, averaging time of 11.6 min and repeat cycle of 1 hour were programmed, each site transmitting while the others were quiet.

[9] HFR's infer the radial current component from the Doppler-shift of radio waves back-scattered by surface gravity waves of half their electromagnetic wavelength (Bragg scattering), or 9.35 m at 16 MHz. Slower wave speeds in shallow water introduce a negligible error (less than 1 cm/s in water deeper than 5 m). Vector currents were estimated on a 5-km Cartesian grid by least squares fitting zonal and meridional components to radial measurements from at least two sites within a 5 km search radius. Poorly constrained estimations were discarded (see Appendix A).

[10] The northernmost site at Faro di Goro, the southern mouth of the Po (44°47.4′N, 12°23.7′E), was operated in beam-forming mode with a linear array of 16 receive antennas oriented at 46° clockwise from north, yielding an azimuthal resolution of ~7 degrees [*Gurgel et al.*, 1999]. The intermediate site at Punta Marina, Ravenna (44°26.8′N, 12°17.6′E), and the southernmost site at Monte San Bartolo, Pesaro (43°56.6′N, 12°50.6′E), were both operated in direction-finding mode with 4 receive antennas in a square array.

[11] The transmit antennas array formed a beam toward the ocean, and a null in the direction of the receive antennas, to reduce the direct path energy. This also reduced the range away from the beam axis, as seen in Figure 1. Ranges increased by ~10 km at night, presumably due to diurnal variations of ionospheric propagation and absorption. This resulted in periodically missing observations at long ranges. While this does not affect the least squares analysis of constituents not synchronous to S_1, it biases that of S_2 and K_1, which differs from S_1 by only 1 cycle/year (see Table 1), and the estimation of power spectra. To alleviate this problem, missing data segments shorter than 16 hours were interpolated (see Appendix B). Temporal coverages of the individual sites and of the vector currents estimations are shown in Figure 2. Data were recorded about 80% of the time.

[12] Data quality can be visualized by the correlation between radial currents from pairs of sites. As shown in Appendix C, the correlation should approach -1 along the baseline joining the two sites, where the radials are in opposite directions, and +1 far offshore, where the radials are almost collinear. If along-baseline and across-baseline current components were uncorrelated with equal variance, the correlation pattern would follow that of the cosine of the angle between the two sites. This relationship is well verified for pairs of sites including the beam-forming radio in Goro (Figure 3, top and middle), but degrades for the pair of direction-finding sites (Figure 3, bottom), reflecting the lower reliability of the direction finding method.

3. Numerical Model

[13] The finite element model of *Janeković and Kuzmić* [2005] is based on the 3-D, nonlinear, shallow water equations [*Lynch et al.*, 1996] with no stratification. The

Table 1. Periods (in Days) Corresponding to the Frequency Difference Between Pairs of Diurnal (Upper Triangle) and Semidiurnal (Lower Triangle) Tidal Constituents

	O_1	P_1	S_1	
	13.7	182.6	365.3	K_1
S_2	14.8	14.8	14.2	O_1
N_2	27.6	9.6	365.2	P_1
K_2	13.7	182.6	9.1	
	M_2	S_2	N_2	

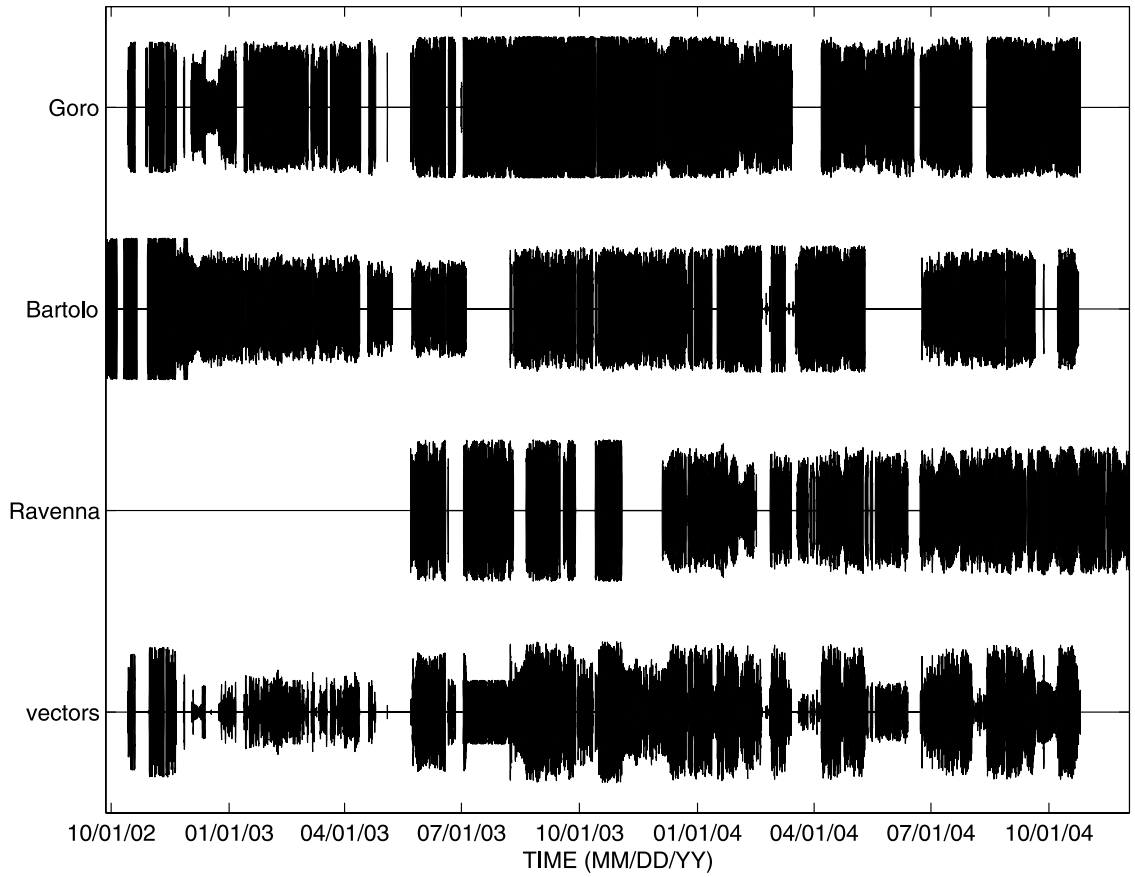

Figure 2. Temporal coverage of individual sites and of the combined vector currents. The thickness corresponds to the percentage of grid points with data. The fraction of time when there is some data over the operating periods is 83.8% for Goro, 79.5% for Pesaro, 80.1% for Ravenna, and 79.4% for the vector currents.

2.5-level turbulence-closure scheme of *Mellor and Yamada* [1982] is used with the improvements of *Galperin et al.* [1988]. The horizontal diffusion parametrization scheme follows *Smagorinsky* [1963]. A free-slip condition is imposed along the coast. Bottom stress is estimated by a quadratic drag law using a coefficient of 0.003. A bathymetry-following coordinate system is used in the vertical, with 21 nonuniformly spaced nodes, providing increased resolution in the surface and bottom layers. The near-surface resolution is 1 m, approximately the effective depth of HFR's measurements [*Stewart and Joy*, 1974]. The finite element grid covers the entire Adriatic Sea from the strait of Otranto at 40°N, with nodal distances ranging from 500 m in coastal areas to 44 km in deep water.

[14] The model is forced by a time-varying sea level boundary condition along 40°N, synthesized for the seven major tidal constituents (M_2, S_2, N_2, K_2, K_1, O_1, P_1) with a 3-D linearized model assimilating coastal sea level observations. This approach is justified by *Janeković et al.* [2003], who confirmed that direct astronomical forcing has a minor effect compared to dominant co-oscillations forced by the Ionian Sea. No observations of currents were used in the assimilation.

[15] The tidal currents parameters were bi-linearly interpolated from the finite-element grid onto the HFR's polar and Cartesian grids, for comparisons with the harmonic analysis of the observed currents.

4. Tidal Currents

[16] The most energetic currents for periods shorter than 5 days are tidal and inertial. Figure 4 shows the average rotary power spectrum over 61 grid points with more than 75% data return. Spectral smearing due to missing observations was minimized (see Appendix B).

[17] The semidiurnal peaks are centered on M_2 and S_2. For M_2, the counterclockwise energy dominates slightly, resulting in highly eccentric counterclockwise current ellipses. On the contrary, for S_2, the clockwise energy dominates. The diurnal peaks are centered on K_1, and a much weaker O_1, both strongly dominated by clockwise energy, resulting in less eccentric clockwise ellipses. The clockwise inertial frequency band (centered on $f_i = (17\ hr)^{-1}$) is unusually broad, possibly frequency-shifted by the vorticity of subinertial currents [*Weller*, 1982; *Kunze*, 1985]; the intermittent forcing by strong Bora wind events is also noted [*Lee et al.*, 2005].

[18] Harmonic analyses of current components (radial, zonal and meridional) were performed with the T-tide Matlab package [*Pawlowicz et al.*, 2002]. Only the 7 tidal constituents modeled by *Janeković and Kuzmić* [2005] were

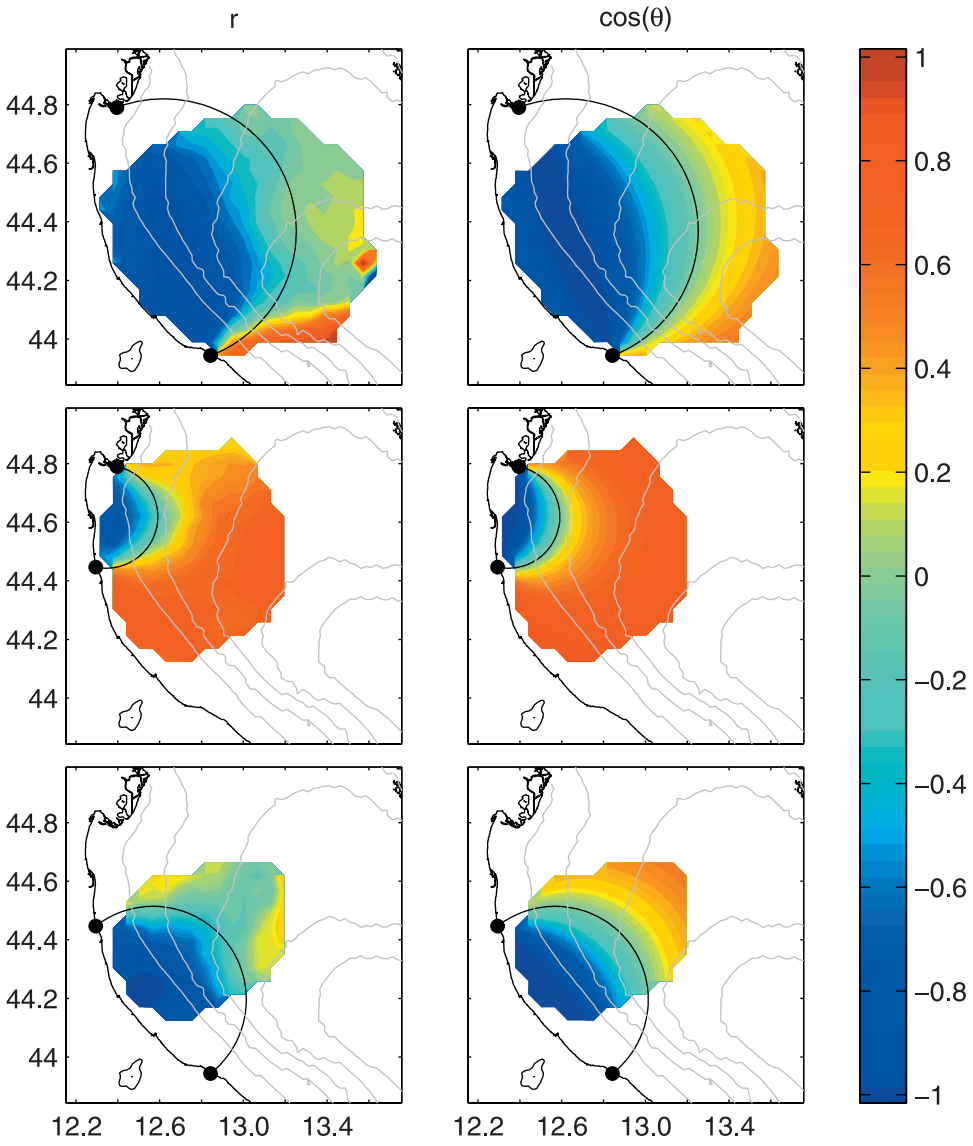

Figure 3. Cross-correlation between radial currents from pairs of sites (left column), and cosine of the angle between the sites (right column), for Goro and Pesaro (top row), Goro and Ravenna (middle row), and Pesaro and Ravenna (bottom row). The circle where the angle between the two sites is 90° is shown for reference.

least squares fitted to the observations, along with a constant and a linear trend; using more constituents degraded the correlation with the model. Nodal corrections were applied for consistency with the model. The 95% confidence intervals were computed by a bootstrap method.

[19] Maps of observed and modeled tidal current ellipses, major axis amplitudes and phases, and their differences are shown in Figure 5 for M_2 and Figure 6 for K_1, and scatterplots of modeled versus observed ellipse parameters are shown in Figure 7. The other modeled constituents have similar patterns within each group, but the observed ones differ from each other. This is due to low signal-to-noise ratios for the weaker constituents (amplitudes are less than 2 cm/s for N_2, K_2, O_1 and P_1). The observed S_2 pattern is similar to the M_2 pattern, but their direction of rotation differs, as noted above.

[20] In the basin interior, M_2 ellipses degenerate into oscillations along the Adriatic axis, consistent with their description as a superposition of Kelvin waves traveling in opposite directions [*Hendershott and Speranza*, 1971; *Mosetti*, 1986]. Their inclination turns with the channel orientation near 44.6°N. Evanescent Poincare waves are suggested by less eccentric ellipses within 20 km from the coast, about the e-folding scale of M_2 Poincare modes [*Hendershott and Speranza*, 1971]. The mostly counterclockwise ellipses rotation is also consistent with Kelvin waves, away from the closed end of the channel [*Taylor*, 1921; *Mosetti*, 1986]. Between Pesaro and Goro, the M_2 major axis amplitudes decrease toward the coast as in *Malačič et al.* [2000]. The model underestimates the amplitudes by 2 cm/s near the coast and overestimates them by 1.5 cm/s in the interior. The M_2 phases are relatively uniform over the width of the basin, consistent with the observations of *Ursella and Gačić* [2001] and with the location of the amphidrome farther south [*Lozano and Candela*, 1995]. In the interior, the observed phases lag

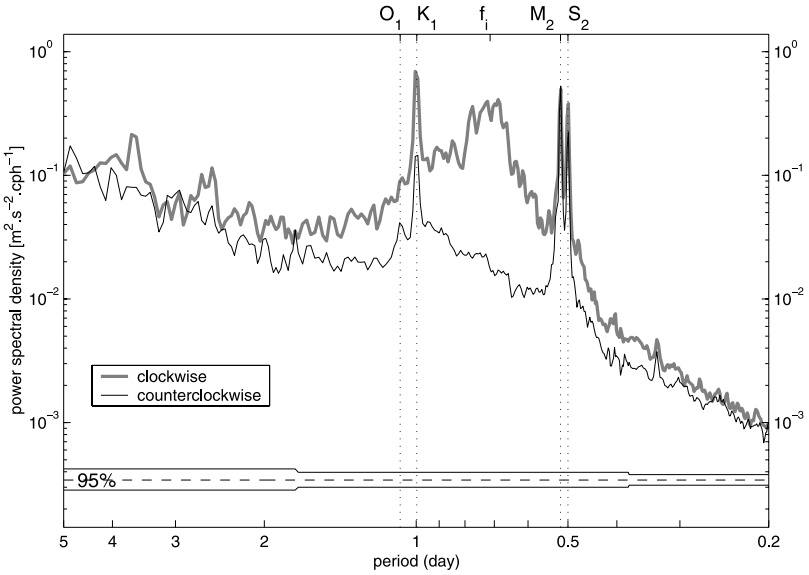

Figure 4. Rotary power spectrum averaged over 61 grid points with more than 75% temporal coverage. 95% confidence interval narrows at higher frequencies with the increased number of degrees of freedom used in the selected frequency ranges. Tidal constituents and inertial frequency f_i are indicated on the top x-axis.

the model phases by 5 to 10 degrees (10 to 20 min.). A peculiar feature of the model, not observed, is the sharp phase decrease within 10-20 km from the coast, where the model lags the observations by up to 50° (1.7 hours).

[21] Modeled K_1 ellipses, major axis amplitudes, and phases patterns mimic those of M_2, suggesting that in this part of the basin K_1 tides may be described as a superposition of Kelvin waves as well. The topographic wave model of *Malačič et al.* [2000] produces an increase of current amplitude toward shallower water, and a lag of the tide along the Italian compared to the Croatian coast. Both model and observations show the opposite here. The along-channel topographic slope is gentler in the northern part of the basin than in the southern part, allowing diurnal tides to propagate as Kelvin waves. The modeled amplitudes underestimate the observed ones by 2 cm/s along the coast and underestimate them by 1.5 cm/s in the interior. The modeled phases lag the observed ones by up to 100° (6.7 hours) along the coast, except south of 44.2°N where observations indicate a decrease in phase at the coast as well. Observed ellipses are less eccentric and veer counterclockwise by ~13°, compared to the modeled ones.

[22] The scatterplots of modeled versus observed ellipse parameters (Figure 7) summarize the comparison. Overall, there is a better agreement for M_2 than for the weaker K_1, as was also noted for comparisons with moored current meters [*Janeković and Kuzmić*, 2005]. All parameters are well correlated, except the minor axes amplitudes, which have low signal-to-noise ratios (see Table 2). This explains the differences in direction of rotation and eccentricity of the K_1 ellipses (Figure 6). The slopes of the major axes amplitudes scatters are greater than 1, a consequence of the modeled values being weaker than the observed ones near the coast but stronger in the interior, as noted above.

[23] Statistics for major axis amplitude and Greenwich phase are condensed in a phase-plane representation in Figure 8 for M_2, K_1, S_2 and O_1. The agreement is good for M_2, S_2 and O_1, but the model lags on average the observations by 15° for K_1. The standard deviations for the model are larger than for the observations, a result of the model behavior near the coast, except for the weaker O_1.

[24] Ellipse parameters for M_2 and K_1 at two ACE (Adriatic Circulation Experiment) moorings (CP2 and CP3, see Figure 1 for their locations) are given in Table 2, and illustrated in Figure 9. Data from the bottom-mounted ACE ADCP's (operational from September 2002 to April 2003) were provided by Jeff Book, and analyzed with T-tide. There is an excellent agreement for M_2 between both instruments and the model at each mooring location, but it is less good for K_1, except for the phases. The HFR's ellipses are much less eccentric than the model and ADCP's ellipses, and Table 2 shows that the minor axes amplitudes are significantly different from zero at 95% confidence for the HFR's. This peculiar feature may be due to a biasing from the diurnal modulation of data coverage, as the moorings lie outside the 50% daytime coverage for Pesaro (Figure 1).

[25] Time series of modeled and observed tidal currents, and of observed total currents, are shown for the fortnight 01/01/2004 to 01/15/2004 in Figure 10 at the grid points closest to moorings CP2 and E4. At CP2, modeled and observed tidal currents are similar in amplitude and phase, while at E4 the observed amplitude is consistently stronger than the modeled one, and the phases are slightly offset. At CP2, the observed current variability is well explained by the phase-locked tides, while at E4 the variability is still dominated by the tides but with stronger amplitudes and phase offsets. This suggests a contribution from non-phase-locked internal tides at E4, where the water column is stratified by fresh surface water from the Po, whereas at CP2, lying in the basin interior, the water column is mixed from surface to bottom during winter [*Rizzoli and Bergamasco*, 1983].

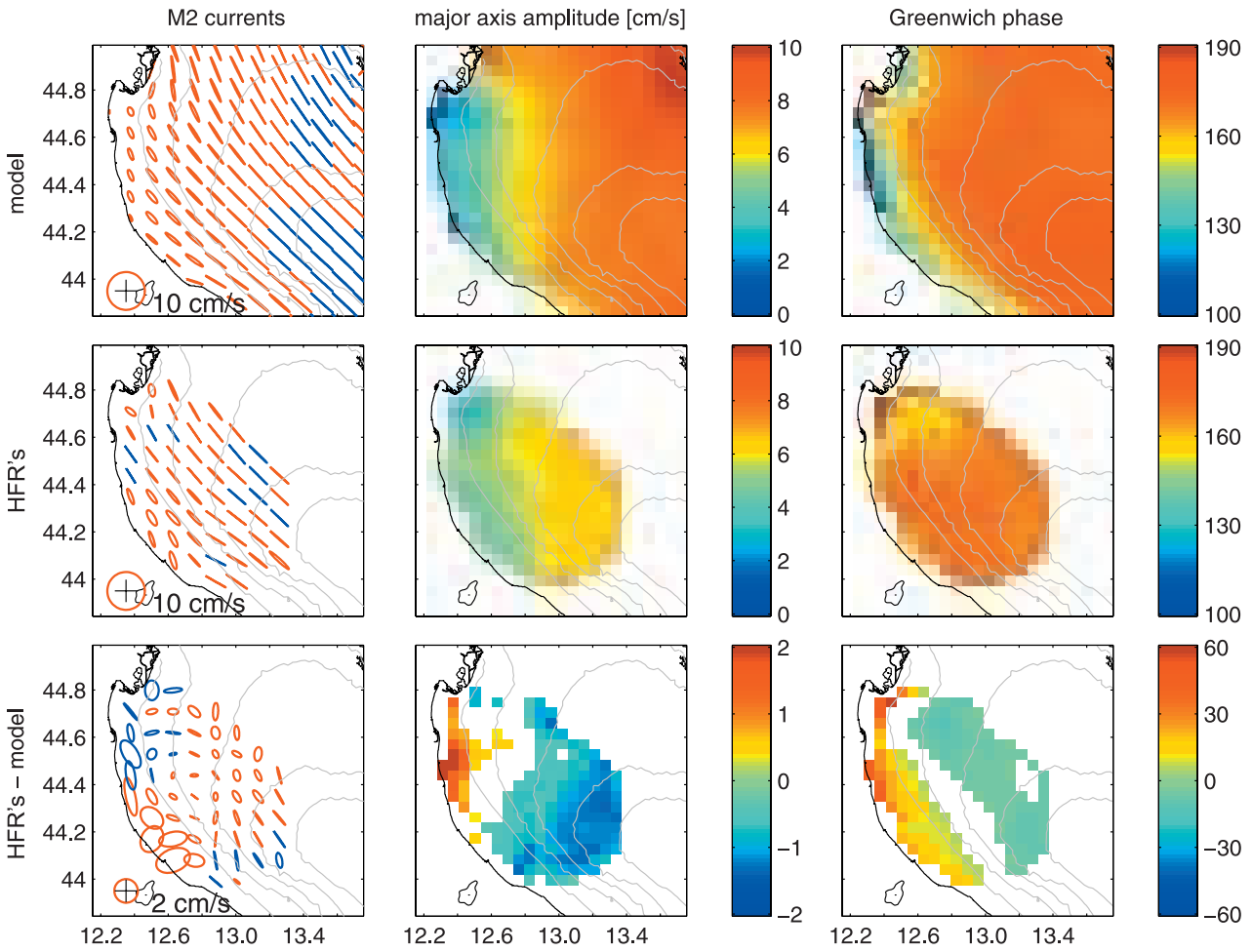

Figure 5. (left column) M_2 ellipses, (middle column) major axis amplitude, and (right column) Greenwich phase from (top row) the model, (middle row) the HFR's, and (bottom row) the difference HFR's - model (shown only where greater in absolute value than the combined 95% confidence intervals from the observations and model error analyses). Counterclockwise and clockwise ellipses are plotted in red and blue, respectively. The phase is defined as the lag of the maximum current (along the northern semimajor axis) with respect to the astronomical phase of M_2 at 0°E.

[26] The major differences between modeled and observed surface tidal currents are thus within a 20-km wide band along the Italian coast. This region is also along the baselines between pairs of sites, yielding poor estimation of the across-baseline (across-shore) current component (see Figure A1). To show that the differences are not due to geometry, the modeled currents were projected onto the radial directions from the HFR's, and compared with the observed radial tidal currents.

[27] Comparisons for M_2 radial amplitude and phase in the directions from Goro and Pesaro are shown in Figures 11 and 12, respectively. The amplitudes decrease and the phases jump by 180° as the radial direction approaches the minor axes orientation. The lag between modeled and observed phases near the coast is similar to the lag for the vector currents, showing that it is not an artifact of the geometric dilution of precision. Furthermore, since the HFR's resolved azimuth through beam-forming at Goro but direction finding at Pesaro, the phase lag is not an artifact of the method of azimuthal resolution.

5. Western Adriatic Current

[28] Phase-locked tidal currents explain less than 2% of the total variance over the 2-year record. Low-frequency currents are stronger than tidal currents, and exhibit temporal and spatial variability that may interact with tidal propagation.

[29] The mean circulation over the 2-year record (Figure 13) consists of a southeastward coastal current, the Western Adriatic Current (WAC), and the northern limb of a cyclonic gyre following the 50 m isobath [*Poulain*, 2001], the Northern Adriatic Filament (NAF [*Mauri and Poulain*, 2001]).

[30] Profiles of the mean alongshore current along two cross-shore transects are shown in Figure 14. Off Ravenna (northern section), the WAC is 40-km wide and reaches a

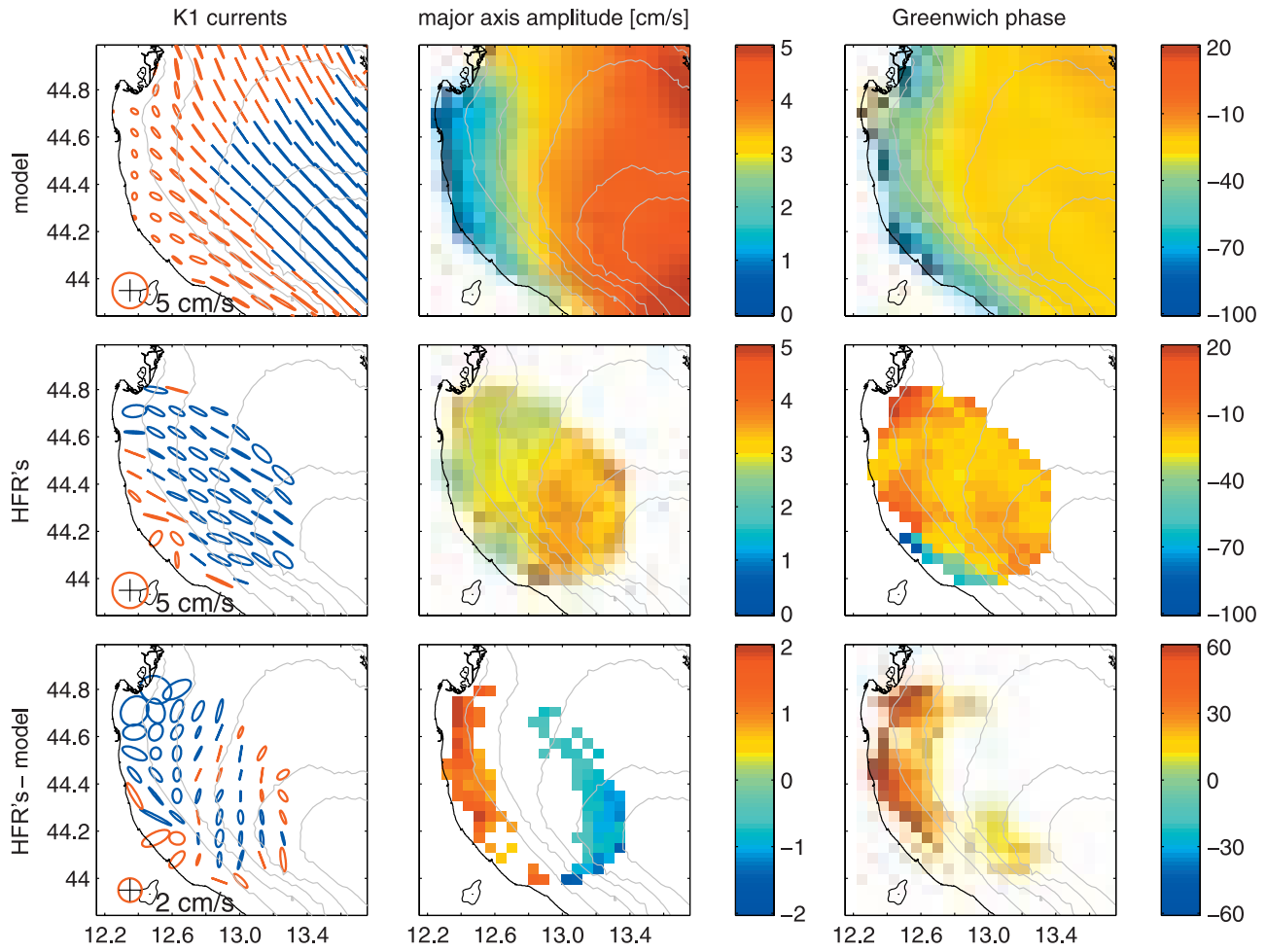

Figure 6. Same as Figure 5 for K_1.

maximum value of ∼6 cm/s at 20 km from the coast. Off Pesaro (southern section), the WAC widens to 50 km and intensifies to 12 cm/s at 10 km from the coast. Its cross-shore profile is almost linear. These characteristics are consistent with those inferred from surface drifters [*Poulain*, 2001]. Neglecting stratification, the mean southward transport at the northern section is ∼0.04 Sv (1 Sv = $10^6 m^3/s$) and increases to ∼0.08 Sv at the southern section, suggesting that as the NAF merges with the WAC, it brings ∼0.04 Sv.

[31] Temporal variability of the WAC is shown in Figure 15. Southeastward currents are intensified during fall/winter and reduced or even reversed during spring/summer, as documented by *Poulain et al.* [2004] for summer 2003. This seasonal cycle is consistent with contemporary surface drifter observations [*Ursella et al.*, 2006]. There are strong high frequency fluctuations, current reversals occurring with periods as short as 3–4 days.

[32] The tides propagate therefore in laterally sheared background currents with spatial scales smaller than tidal wavelengths, and temporal variability from a few days to seasonal.

6. Discussion

[33] The differences between model and observations of tidal currents along the Italian coast are robust features that do not result from measurement limitations, and may be attributed to physical processes absent from the model, or incomplete parametrization of subgrid-scale processes, such as vertical mixing or bottom friction.

[34] The drag coefficient parametrizing bottom friction is constant, but should vary between the smoother muddy bottom along the Italian coast, and the rougher sandy bottom along the Croatian coast [*Brambati*, 1990, Figure 15]. Friction may therefore be overestimated along the Italian coast, reducing the tidal energy there.

[35] Stratification may also account for the differences between model and observations for the super-inertial M_2 tides, by allowing the generation and propagation of internal tides, as the flow oscillates over sloping topography. Even for the subinertial K_1 tides, stratification could be important, if forced baroclinic modes modify significantly the bottom currents, hence the effect of bottom friction. Stratification is strongest in spring and summer, when fresh water spreads from the Po over the northern Adriatic. It disappears during fall and winter in the interior of the basin where the water column is mixed to the bottom by outbreaks of cold dry Bora winds, but persists near the Italian coast along which the Po outflow is confined [*Rizzoli and Bergamasco*, 1983]. This may explain why model and observations compare better in the interior than along the coast. Bottom-mounted

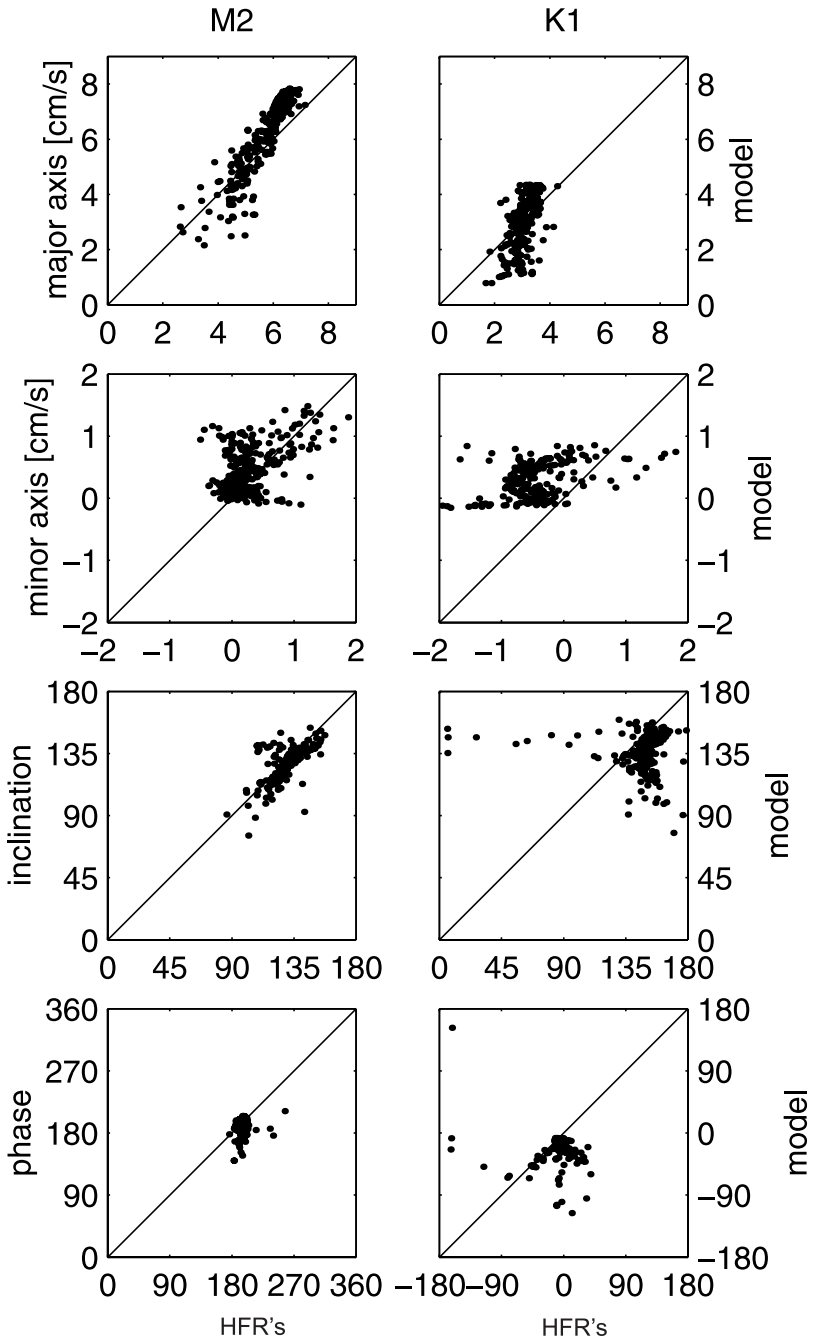

Figure 7. Scatterplots of model (vertical axes) versus HFR's (horizontal axes) tidal ellipse parameters: (top row) major axis amplitude (cm/s), (middle-top row) minor axis amplitude (cm/s, negative values indicate clockwise rotation), (middle-bottom row) inclination (degrees counterclockwise from east), and (bottom row) Greenwich phase (degrees) for M_2 (left column) and K_1 (right column) constituents.

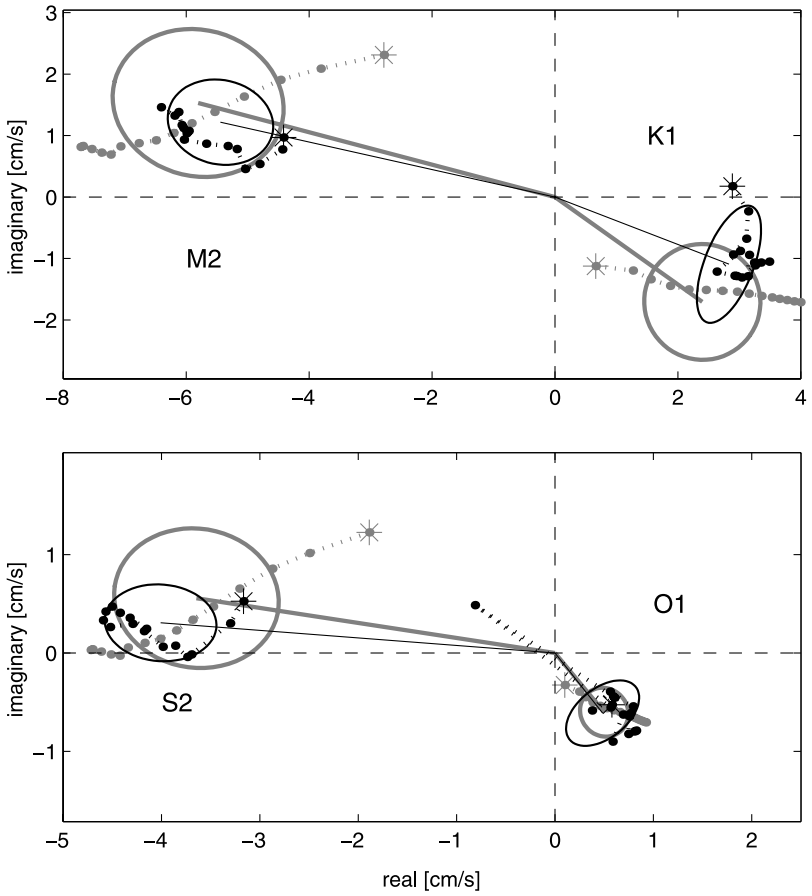

Figure 8. Statistics for the observed (black) and modeled (gray) major axis amplitude (radius) and Greenwich phase (angle) for the four major tidal constituents (top: M_2 and K_1, bottom: S_2 and O_1). The average and standard deviation of amplitudes and phases over the grid points with more than 4383 hourly observations (182.6 days) are represented by solid lines drawn from the origin and by ellipses, respectively. A zonal section along 44.3N is shown by dots, starting from the coast (star).

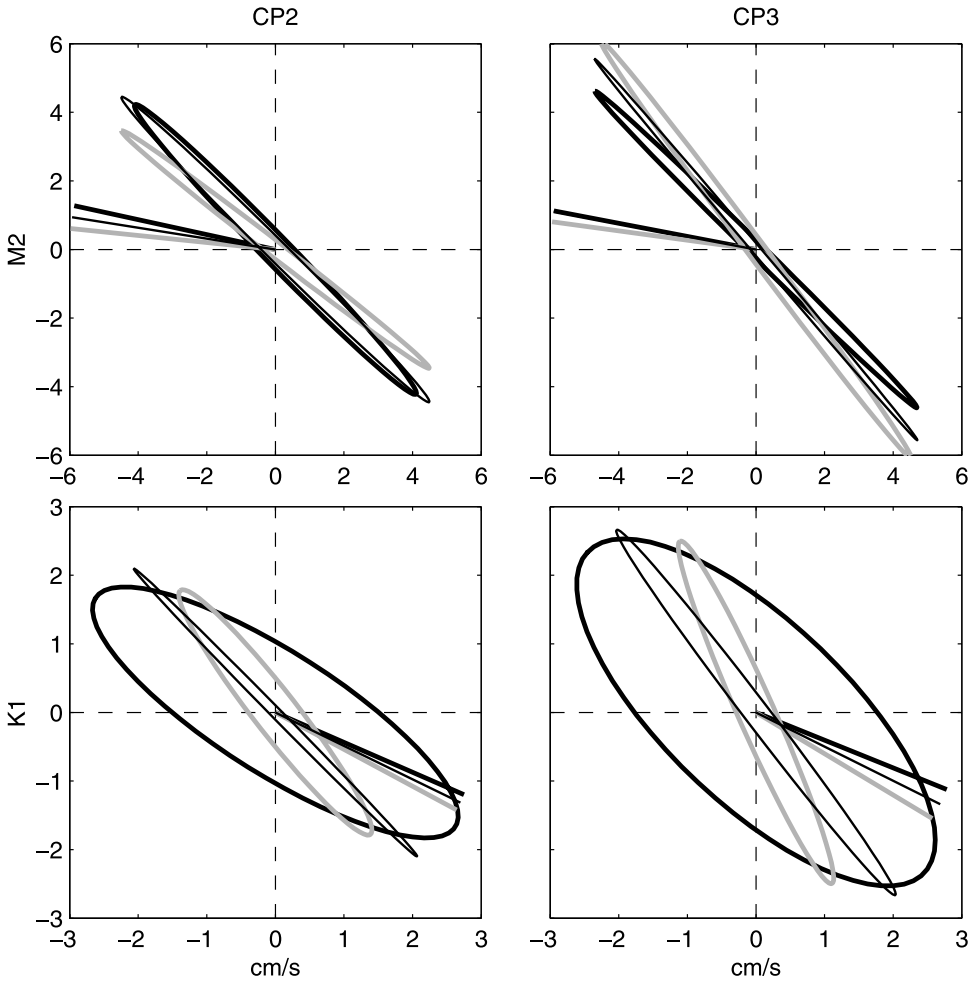

Figure 9. M_2 (top) and K_1 (bottom) current ellipses and Greenwich phases (represented by the angle of the straight lines relative to the x-axis) at the CP2 (left) and CP3 (right) mooring locations. Currents from HFR's (thick black lines), ADCP's at 3.4 m depth (thick gray lines), and model near the surface (thin black lines) are shown.

Table 2. M_2 and K_1 Major and Minor Axes Amplitudes (cm/s), Northern Semimajor Axis Inclination (Degrees Counterclockwise From East), and Greenwich Phase (Degrees) at ACE Moorings CP2 and CP3 (See Figure 1 for Their Locations)[a]

		M_2				K_1			
		maj	min	inc	pha	maj	min	inc	pha
	R	5.9 ± 0.3	0.4 ± 0.4	134.2 ± 3.0	167.8 ± 3.7	3.1 ± 0.5	−0.9 ± 0.5	147.5 ± 12.2	336.5 ± 12.1
CP2	A	5.7 ± 0.5	0.2 ± 0.5	142.4 ± 5.3	174.1 ± 5.7	2.3 ± 0.9	−0.3 ± 0.9	127.9 ± 22.2	331.7 ± 27.0
	M	6.3 ± 0.1	0.3 ± 0.1	135.2 ± 0.8	171.0 ± 0.8	2.9 ± 0.1	−0.1 ± 0.1	134.5 ± 2.1	334.0 ± 2.2
	R	6.6 ± 0.3	−0.2 ± 0.3	135.5 ± 2.4	169.2 ± 2.6	3.4 ± 0.6	−1.3 ± 0.5	136.3 ± 10.9	338.0 ± 10.9
CP3	A	7.6 ± 0.3	−0.3 ± 0.3	126.6 ± 2.9	172.3 ± 2.8	2.7 ± 0.6	−0.3 ± 0.6	113.9 ± 10.4	329.0 ± 14.5
	M	7.3 ± 0.1	0.1 ± 0.1	130.3 ± 0.8	169.4 ± 0.9	3.4 ± 0.1	−0.2 ± 0.1	127.4 ± 1.8	333.6 ± 2.2

[a]R, HFR's observations; A, ADCP observations (at 3.4 m depth); M, model predictions near the surface. The 95% confidence intervals are indicated.

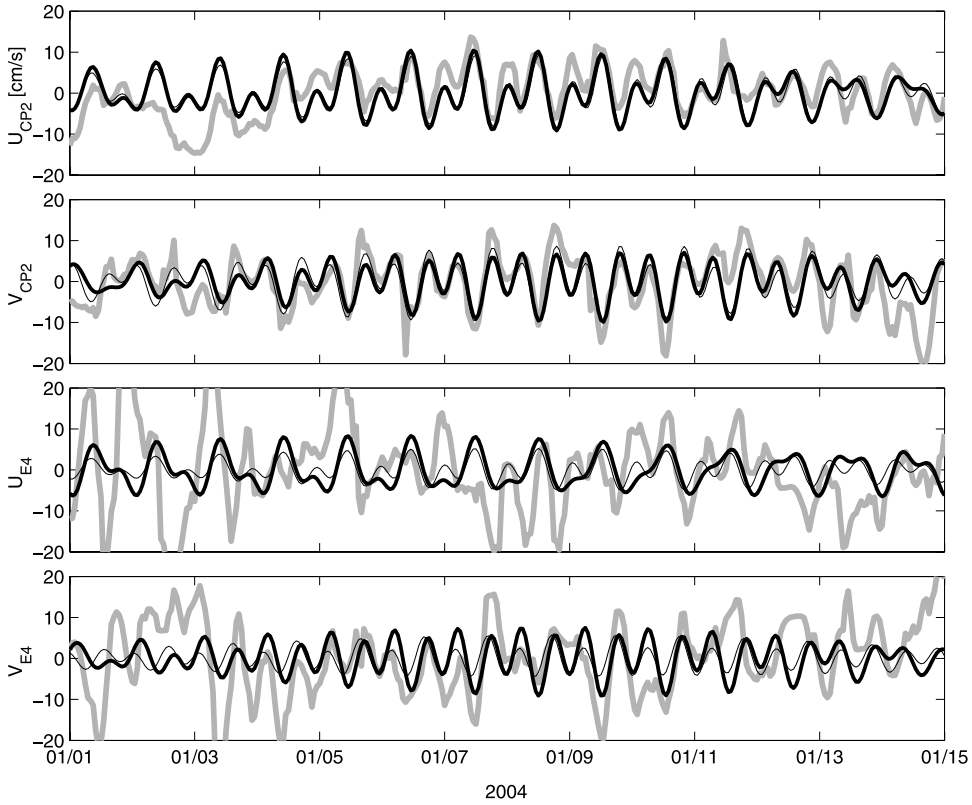

Figure 10. Time series of modeled (thin) and observed (thick black) tidal currents, as well as observed total currents (thick gray) at the grid points closest to moorings CP2 and E4. (top) Zonal current at CP2, (middle-top) meridional current at CP2, (middle-bottom) zonal current at E4, (bottom) meridional current at E4. The mean over the fortnight has been removed from the total currents to improve the comparison.

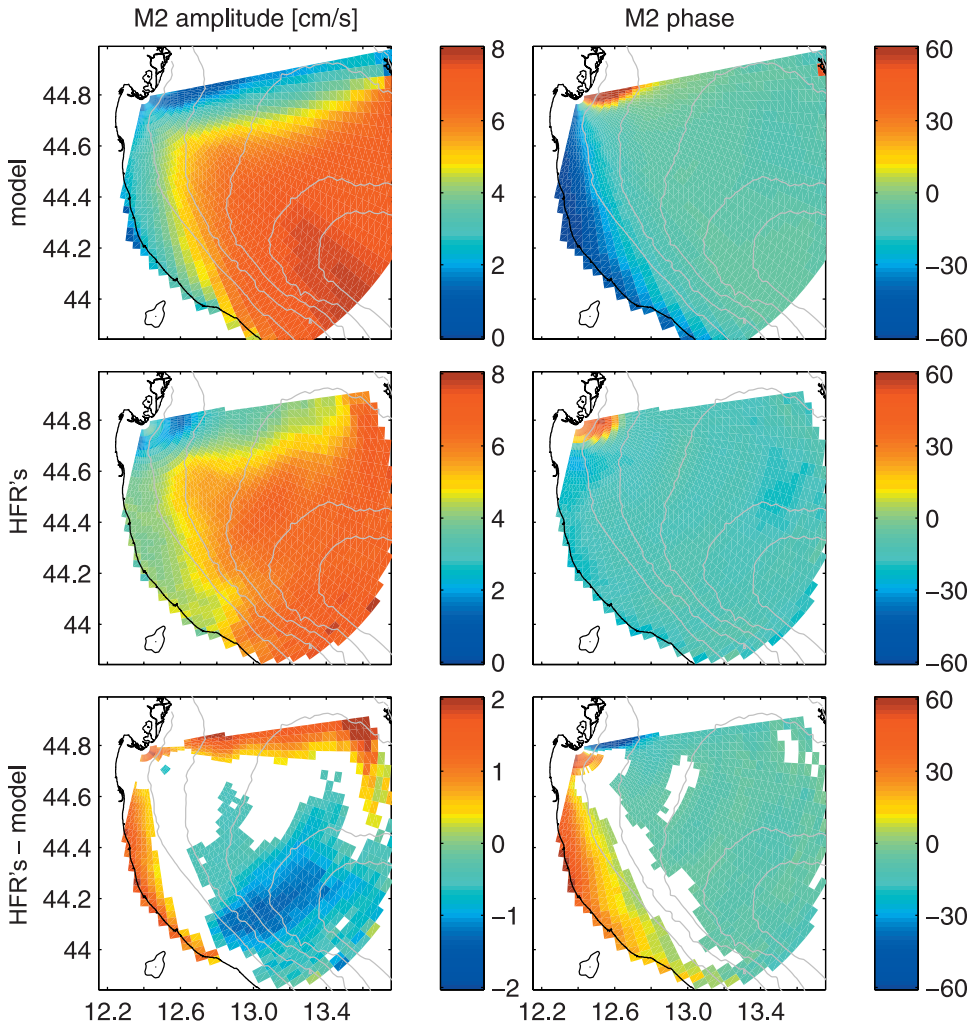

Figure 11. M_2 Goro radial currents amplitude (left column) and phase (right column) from the model (top row), the HFR's (middle row), and the difference HFR's-model (bottom row). The phase is defined as the lag of the maximum radial current with respect to the astronomical phase of M_2 at 0°E.

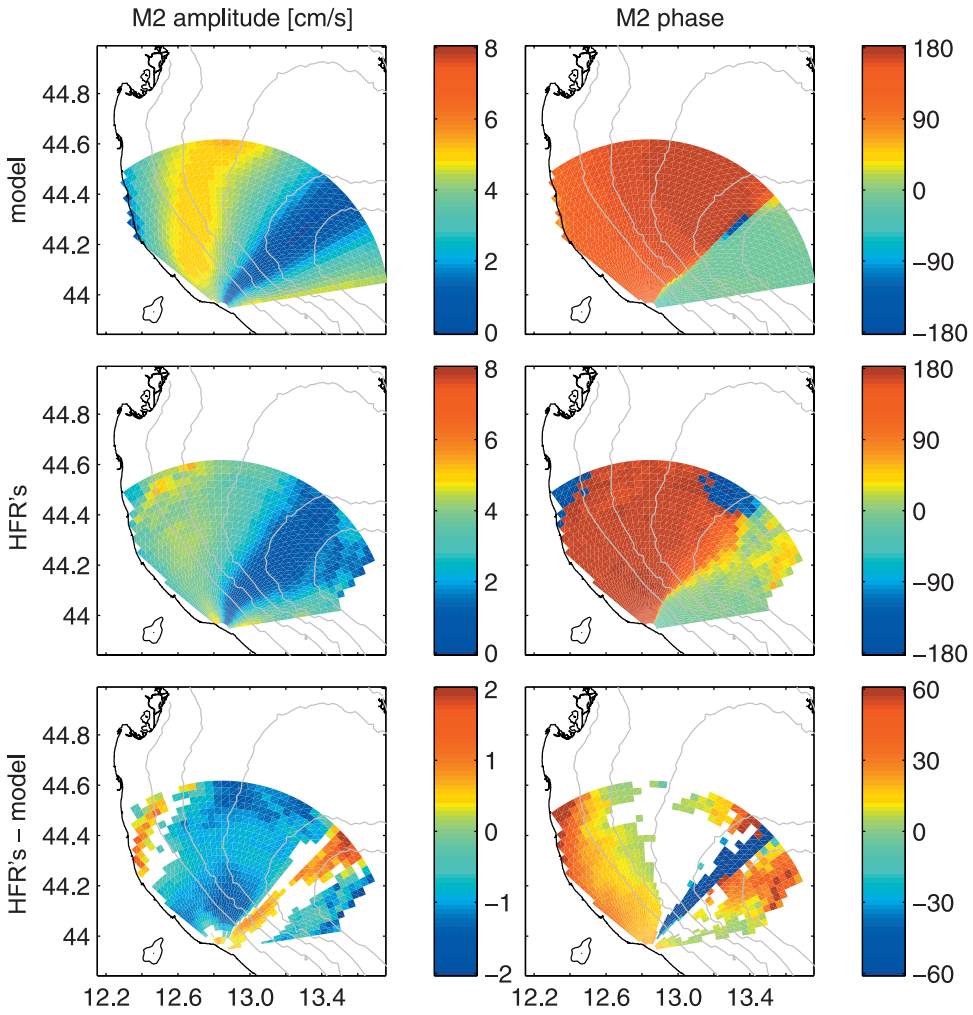

Figure 12. Same as Figure 11 for Pesaro.

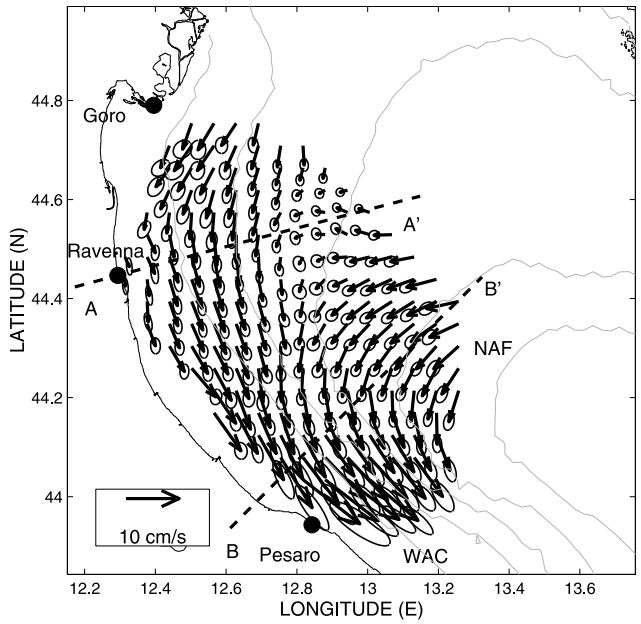

Figure 13. Mean flow over the 2-year record, along with 95% confidence ellipses, computed from the low-pass filtered currents variance scaled by the number of degrees of freedom estimated from the integral timescales of the time series. (Dashed lines) transects AA' and BB' along which mean flow profiles are shown in Figure 14.

ADCP's deployed off the Po delta may help evaluate the internal tides contribution.

[36] Interactions between tidal and low-frequency currents are also absent in the model. Mesoscale currents in the Adriatic will affect the spatial structure and frequency of the normal modes of the basin, since they will affect the propagation of the free waves of the system. Therefore the response of the basin to the periodic tidal forcing at the open boundary should be sensitive to the presence of mesoscale currents, especially if the forcing frequency is very close to an eigenfrequency of the basin, leading to resonance. This is almost the case for the Adriatic, for which the principal modes have periods of 22 hrs and 11 hrs, which explains why the northern Adriatic tides are the second highest tides in the Mediterranean Sea [*Cushman-Roisin et al.*, 2001]. Therefore a possible significant impact of low-frequency currents, even though they are small compared to Kelvin waves propagation speed, cannot be ruled out.

7. Conclusion

[37] Surface tidal currents in the northwestern Adriatic were extracted from HFR time series, and compared with numerical model predictions. The good agreement in the basin interior gives confidence in the model simulations there.

[38] However M_2 and K_1 modeled amplitudes are underestimated by 2 cm/s, and modeled phases significantly lag observed phases in a narrow strip along the coast. This region, less than 30-m deep, is stratified by low-salinity water from the Po outflow, and laterally sheared by the Western Adriatic Current, both absent from the model but possibly affecting tidal propagation. The model may also incompletely parameterize the combined effects of bottom friction and vertical mixing of momentum.

Appendix A: Vector Currents Estimation

[39] Vector currents were estimated on a 5-km Cartesian grid by least squares fitting zonal and meridional components to all radial measurements from at least two sites within a 5-km search radius [*Lipa and Barrick*, 1983;

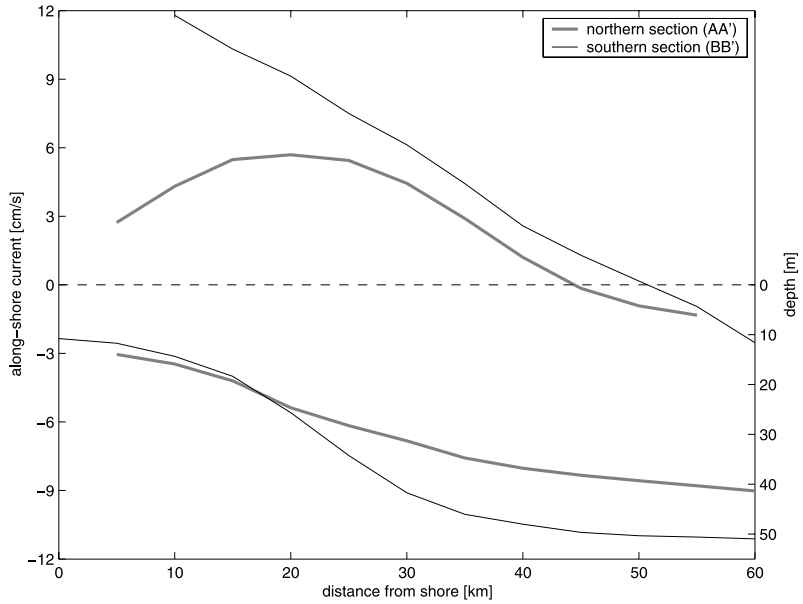

Figure 14. Alongshore component of the mean flow (top curves, left y-axis, positive values indicate flow toward the southeast), and bathymetry (bottom curves, right y-axis), along cross-shore transects AA' and BB' of Figure 13.

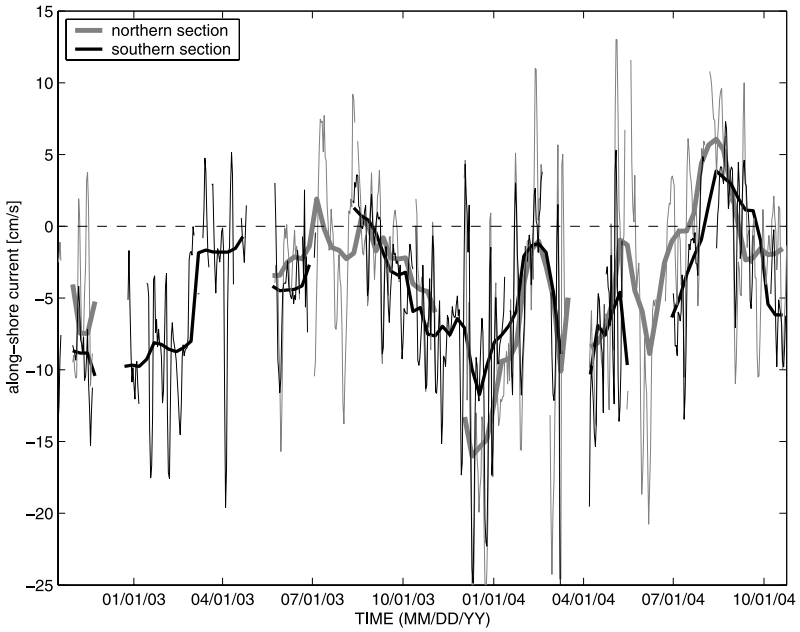

Figure 15. Time series of alongshore flow (negative values indicate flow toward the southeast) averaged over the cross-shore sections shown in Figure 13 from the coast to the distance of no mean flow. Currents were detided and low-pass filtered with a 3-day running median (thin lines), and further low-pass filtered with a 30-day running median (thick lines).

Paduan and Cook, 2004]. The normal component is poorly constrained near the baseline between two sites and the azimuthal component is poorly constrained far from the sites, yielding a Geometric Dilution Of Precision (GDOP [*Chapman et al.*, 1997]). It can be estimated as follows [*Gurgel*, 1994; D. Barrick, unpublished note, 2002].

[40] The current is assumed to be constant within the search radius, where N radial measurements are available:

$$m_i = n_{ix}u + n_{iy}v + e_i \qquad i = 1, ..., N \tag{A1}$$

or

$$\mathbf{m} = \mathbf{N}\mathbf{w} + \mathbf{e} \tag{A2}$$

where $\mathbf{m}$ is the $N \times 1$ vector of radial measurements, $\mathbf{N}$ the $N \times 2$ matrix of the unit radial vectors, $\mathbf{w} = [u, v]^T$ the current vector, and $\mathbf{e}$ the $N \times 1$ vector of measurements noise and model errors.

[41] An estimate of $\mathbf{w}$ can be obtained by minimizing the sum of squared errors:

$$J = \sum_{i=1}^{N} e_i^2 = \mathbf{e}^T\mathbf{e} \tag{A3}$$

[42] The solution is [e.g., *Wunsch*, 2006, pp. 43–46]:

$$\tilde{\mathbf{w}} = \left(\mathbf{N}^T\mathbf{N}\right)^{-1}\mathbf{N}^T\mathbf{m} \tag{A4}$$

provided that $\left(\mathbf{N}^T\mathbf{N}\right)^{-1}$ exists.

[43] The covariance of $\tilde{\mathbf{w}}$ is:

$$\begin{aligned}\mathbf{C}_{\tilde{\mathbf{w}}\tilde{\mathbf{w}}} &= \left\langle (\tilde{\mathbf{w}} - \langle\tilde{\mathbf{w}}\rangle)(\tilde{\mathbf{w}} - \langle\tilde{\mathbf{w}}\rangle)^T \right\rangle \\ &= \left(\mathbf{N}^T\mathbf{N}\right)^{-1}\mathbf{N}^T\mathbf{C}_{\mathbf{ee}}\mathbf{N}\left(\mathbf{N}^T\mathbf{N}\right)^{-1}\end{aligned} \tag{A5}$$

where brackets indicate ensemble averaging, and $\mathbf{C}_{\mathbf{ee}} = \left\langle (\mathbf{e} - \langle\mathbf{e}\rangle)(\mathbf{e} - \langle\mathbf{e}\rangle)^T \right\rangle$ is the covariance of $\mathbf{e}$.

[44] If the errors are independent of each other and have the same variance σ^2, then:

$$\mathbf{C}_{\mathbf{ee}} = \sigma^2\mathbf{I} \tag{A6}$$

where $\mathbf{I}$ is the unit matrix.

[45] The covariance of $\tilde{\mathbf{w}}$ becomes:

$$\mathbf{C}_{\tilde{\mathbf{w}}\tilde{\mathbf{w}}} = \sigma^2\left(\mathbf{N}^T\mathbf{N}\right)^{-1} \tag{A7}$$

[46] This expression for $\sigma = 1$ is the GDOP. The principal axes of $\mathbf{C}_{\tilde{\mathbf{w}}\tilde{\mathbf{w}}}$ are shown in Figure A1 for different geometric configurations. With only two sites, the vector currents cannot be estimated reliably over large areas. A third site is then needed to improve vector currents estimation.

[47] In the present processing, currents were discarded when the largest eigenvalue of $\mathbf{C}_{\tilde{\mathbf{w}}\tilde{\mathbf{w}}}$ exceeded 0.5, and were instead bilinearly interpolated from neighboring grid points. This rather restrictive value was chosen because the errors of neighboring measurements from the same instrument are not truly independent.

Appendix B: Temporal Interpolation and Spectral Estimation

[48] The diurnal modulation of data coverage biases the estimation of power spectra and least squares analysis of constituents synchronized with or not separable from S_1, such as S_2 and K_1, which differs from S_1 by only 1 cycle per year (see Table 1).

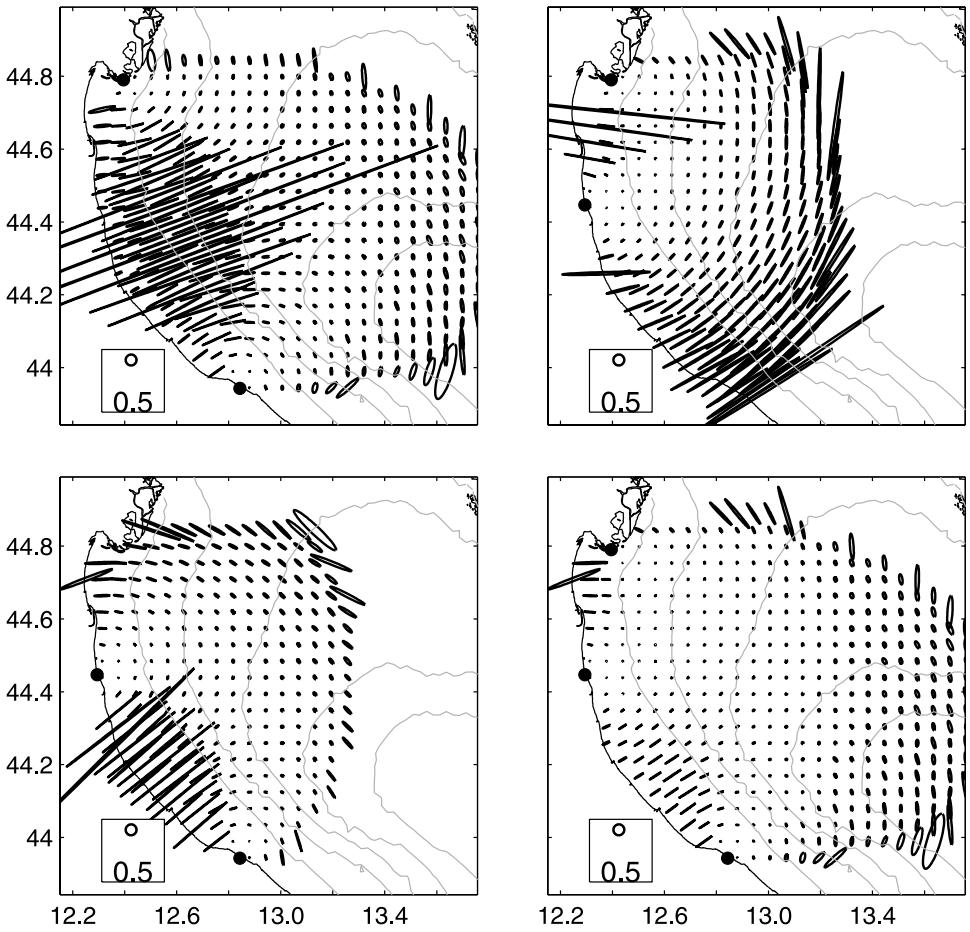

Figure A1. Geometric Dilution Of Precision (GDOP) ellipses for various geometric configurations: (top left) Goro and Pesaro only, (top right) Goro and Ravenna only, (bottom left) Ravenna and Pesaro only, (bottom right) Goro, Ravenna and Pesaro. The legend corresponds to the threshold value selected to discard vector currents poorly constrained.

[49] Most missing data segments are shorter than a day, but long enough to preclude linear interpolation. The main variability for periods shorter than a day is tidal (M_2 and K_1) and inertial with a period of 17 hours at 44.5N. A constant and sinusoids at M_2, K_1 and inertial frequencies were least squares fitted to the observations available in a 3-day window centered on each missing data segment shorter than 16 hours. The fit was performed only if more than 24 observations were available. A linear trend was added to match the interpolation with the observations on the edges of each segment. This interpolation was carried out on the radial and vector currents separately. Vector currents were not estimated from the interpolated radial currents, to avoid spurious tidal variability arising from geometric dilution of precision (see Appendix A). The least squares analysis was carried on the interpolated time series.

[50] To estimate the power spectra of the time series, their mean was removed and the remaining missing data segments were replaced by zeros. This amounts to multiplying the uninterrupted signal by a missing data function (1 for data and 0 for no data). In the frequency domain, the Fourier transform of the uninterrupted signal is convoluted with the Fourier transform of the missing data function, resulting in spectral smearing. To minimize such smearing, continuous data segments shorter than 36 hours were replaced by zeros, and the spectrum was estimated only when data return was greater than 75%. Time series were multiplied by a Blackman window prior to computing their Fourier transform. The spectrum shown in Figure 4 is an average of the spectra at 61 grid points. The 95% confidence intervals are based on an effective number of degrees of freedom of 61/4, since adjacent grid points are not independent of each other. The number of degrees of freedom was increased for higher frequencies, by splitting the time series into half-overlapping segments. Each segment was demeaned and multiplied by a Blackman window.

Appendix C: Radial Currents Cross-Correlation

[51] The components u and v of vector current along and normal to the baseline between two sites (line joining the two sites) are:

$$\begin{cases} u(t) = V(t)\cos\theta(t) \\ v(t) = V(t)\sin\theta(t). \end{cases} \tag{C1}$$

where V and θ are the vector current magnitude and angle relative to the baseline.

[52] Radial currents in the directions from the sites can be expressed at a particular location by:

$$\begin{cases} v_1(t) = V(t)\cos(\theta(t) - \theta_1) \\ v_2(t) = V(t)\cos(\theta(t) - \theta_2). \end{cases} \tag{C2}$$

where θ_1 and θ_2 are the directions of the radial components relative to the baseline.

[53] The radial currents cross-correlation coefficient is:

$$r_{12} = \frac{\langle v_1 v_2 \rangle}{\sqrt{\langle v_1^2 \rangle \langle v_2^2 \rangle}} \tag{C3}$$

where brackets indicate time averaging.

[54] The covariance and variances of the radial currents can be expressed in terms of the covariance and variances of u and v:

$$\begin{aligned} \langle v_i v_j \rangle = {} & \frac{1}{2}\langle u^2 + v^2 \rangle \cos(\theta_i - \theta_j) \\ & + \langle uv \rangle \sin(\theta_i + \theta_j) \\ & + \frac{1}{2}\langle u^2 - v^2 \rangle \cos(\theta_i + \theta_j) \qquad (i,j) = (1,2) \end{aligned} \tag{C4}$$

[55] Along the baseline, $\theta_1 = 0$ and $\theta_2 = \pi$, yielding $r_{12} = -1$. Far from the sites, $\theta_1 \to \frac{\pi}{2}$ and $\theta_2 \to \frac{\pi}{2}$, yielding $r_{12} \to +1$.

[56] If u and v are uncorrelated and have the same variance, then

$$\langle v_i v_j \rangle = \frac{1}{2}\langle u^2 + v^2 \rangle \cos(\theta_i - \theta_j) \qquad (i,j) = (1,2) \tag{C5}$$

yielding

$$r_{12} = \cos(\theta_1 - \theta_2) \tag{C6}$$

[57] **Acknowledgments.** The authors thank Eric Firing, Douglas Luther, Paola Malanotte-Rizzoli, and Mark Merrifield for fruitful scientific discussions, and Jeff Book for providing the ADCP's data. The comments of two anonymous reviewers contributed significantly to improve the manuscript. Olivier Ali, Jérôme Aucan, Riccardo Barbanti, Joël Benito, Fabio Brunetti, Alessandro Bubbi, Roberto Cecco, Julie Degoulet, Sophie Delambert, Davide Deponte, Michele Deponte, Julie Deshayes, Adrien Desoria, Bénédicte Dousset, Io Flament, Maël Flament, Monika Hamann, Thomas Helzel, Matthias Kniephoff, Oliver Koshe, Paolo Mansutti, Elena Mauri, Kimball Millikan, Philip Moravcik, Giulio Notarstefano, Georges Peeters, and Derek Young helped with HFR's installation and maintenance, and with data processing. Yves Barbin provided numerous suggestions on operating and calibrating the instruments, and Pierre Broche processed some data with the MUSIC direction finding algorithm to compare with our least squares fit algorithm, with satisfactory results. The HFR radar processing routines by Jeff Paduan and Mike Cook were adapted to compute the vector currents from the radial measurements. Administrative assistance was provided by Gina Constantini, Laura Glenn and Lance Samura. We are grateful to the following individuals and institutions for providing permits and for helping with logistics: Monte San Bartolo: Ente Parco Naturale Monte San Bartolo, Provincia di Pesaro Urbino, Comune di Pesaro, Comando 28Regg. Fant. Pavia, ARPAM Pesaro, Dr. F. Piperno; Faro di Goro: Consorzio per la Gestione del Parco Regionale del Delta del Po, Comune di Goro, Provincia di Ferrara, Corpo Forestale dello Stato, Fabrizio Farinelli and Valentino Gianella; Punta Marina: Capitaneria di Porto di Ravenna, Agenzia delle Dogane, AGIP Petroli, ARPA Ravenna. Support was obtained from the following funding agencies: the United States Office of Naval Research (grants N00014-02-1-0272 to P. Flament and N00014-03-1-0291 to P.-M. Poulain), the United States National Science Foundation (grants OCE-9724464 and OCE-0453848 to P. Flament), the Italian Consiglio Nazionale delle Ricerche, the Croatian Ministry of Science, Education and Sports (grant 0098113 to M. Kuzmić and I. Janeković. P. Flament is partially supported by the state of Hawaii. Contribution 6733 from the School of Ocean and Earth Science and Technology, University of Hawaii.

References

Brambati, A. (1990), Origin and evolution of the Adriatic Sea, paper presented at 25th Eur. Mar. Biol. Symp., Univ. of Ferrara, Ferrara, Italy.

Cavallini, F. (1985), A three-dimensional numerical model of tidal circulation in the northern Adriatic Sea, *Boll. Oceanol. Teor. Appl.*, *III*(3), 205–218.

Chapman, R. D., L. K. Shay, H. C. Graber, J. B. Edson, A. Karachintsev, C. L. Trump, and D. B. Ross (1997), On the accuracy of HF radar surface current measurements: Intercomparisons with ship-based sensors, *J. Geophys. Res.*, *102*(C8), 18,737–18,748.

Cushman-Roisin, B., and C. E. Naimie (2002), A 3d finite-element model of the Adriatic tides, *J. Mar. Syst.*, *37*, 279–297.

Cushman-Roisin, B., V. Malačič, and M. Gačić (2001), Tides, seiches and low-frequency oscillations, in *The Physical Oceanography of the Adriatic Sea: Past, Present and Future*, pp. 217–240, Springer, New York.

Defant, A. (1914), Zur theorie der gezeiten im adriatischen meere, *Ann. Hydrogr. Mar. Meteorol.*, *42*, 270–281.

Galperin, B., L. H. Kantha, S. Hassid, and A. Rosati (1988), A quasi-equilibrium turbulent energy model for geophysical flows, *J. Atmos. Sci.*, *45*, 55–62.

Gurgel, K.-W. (1994), Shipborne measurement of surface current fields by HF radar, *L'Onde Electrique*, *74*(5), 54–59.

Gurgel, K.-W., G. Antonischki, H.-H. Essen, and T. Schlick (1999), Wellen Radar (WERA): A new ground-wave HF radar for ocean remote sensing, *Coastal Eng.*, *37*, 219–234.

Hendershott, M. C., and A. Speranza (1971), Co-oscillating tides in long, narrow bays; the Taylor problem revisited, *Deep Sea Res.*, *18*, 959–980.

Janeković, I., and M. Kuzmić (2005), Numerical simulation of the Adriatic Sea principal tidal constituents, *Ann. Geophys.*, *23*, 1–12.

Janeković, I., J. Bobanoviæ, and M. Kuzmić (2003), The Adriatic Sea M2 and K1 tides by 3D model and data assimilation, *Estuarine Coastal Shelf Sci.*, *57*, 873–885.

Kunze, E. (1985), Near-inertial wave propagation in geostrophic shear, *J. Phys. Oceanogr.*, *15*, 544–565.

Lee, C. M., et al. (2005), Northern Adriatic response to a wintertime bora wind event, *Eos Trans. AGU*, *86* (16), 157, 163, 165.

Lipa, B. J., and D. E. Barrick (1983), Least squares methods for the extraction of surface currents from codar crossed-loop data: Application at ARSLOE, *IEEE J. Oceanic Eng.*, *8*, 226–253.

Lozano, C. J., and J. Candela (1995), The M2 tide in the Mediterranean Sea: Dynamic analysis and data assimilation, *Oceanol. Acta*, *18*(4), 419–441.

Lynch, D. R., T. C. I. P. Justin, C. E. Naimie, and F. E. Werner (1996), Comprehensive coastal circulation model with application to the Gulf of Maine, *Cont. Shelf Res.*, *16*, 875–906.

Malačič, V., D. Viezzoli, and B. Cushman-Roisin (2000), Tidal dynamics in the northern Adriatic Sea, *J. Geophys. Res.*, *105*(C11), 26,265–26,280.

Mauri, E., and P.-M. Poulain (2001), Northern Adriatic Sea surface circulation and temperature/pigment fields in september and october 1997, *J. Mar. Syst.*, *29*, 51–67.

Mellor, G. L., and T. Yamada (1982), Development of a turbulence closure model for geophysical fluid problems, *Rev. Geophys.*, *20*, 851–875.

Michelato, A. (1983), Caratteristiche della circolazione delle acque costiere dell'Emilia-Romagna, in *Atti del Convegno "Eutrofizzazione dell'Adriatico-Ricerche e linee di intervento,"* pp. 149–168, Bologna, Italy.

Mosetti, R. (1986), Determination of the current structure of the M2 tidal component in the northern Adriatic by applying the rotary analysis to the Taylor problem, *Boll. Oceanol. Teor. Appl.*, *IV*(3), 165–172.

Orlić, M., M. Gačić, and P. E. L. Violette (1992), The currents and circulation of the Adriatic Sea, *Oceanol. Acta*, *15*(2), 109–124.

Paduan, J., M. Cook, (2004), HFRadarmap toolbox for MATLAB, Nav Postgrad. Sch., Monterey, Calif. (Available at http://www.oc.nps.navy.mil/radlab/HFRadarmapToolbox/)

Pawlowicz, R. B., B. Beardsley, and S. Lentz (2002), Classical tidal harmonic analysis including error estimates in MATLAB using T_TIDE, *Comput. Geosci.*, *28*, 929–937.

Poulain, P.-M. (2001), Adriatic Sea surface circulation as derived from drifter data between 1990 and 1999, *J. Mar. Syst.*, *29*, 3–32.

Poulain, P.-M., E. Mauri, and L. Ursella (2004), Unusual upwelling event and current reversal off the Italian Adriatic coast in summer 2003, *Geophys. Res. Lett.*, 31, L05303, doi:10.1029/2003GL019121.

Rizzoli, P. M., and A. Bergamasco (1983), The dynamics of the coastal region of the northern Adriatic Sea, *J. Phys. Oceanogr.*, *13*, 1105–1130.

Smagorinsky, J. (1963), General circulation experiments with the primitive equations. I: The basic experiment, *Mon. Weather Rev.*, *91*, 99–164.

Stewart, R. H., and J. W. Joy (1974), HF radio measurements of surface currents, *Deep Sea Res.*, *21*, 1039–1049.

Taylor, G. I. (1921), Tidal oscillations in gulfs and rectangular basins, *Proc. London Math. Soc.*, *20*, 193–204.

Ursella, L., and M. Gačić (2001), Use of the Acoustic Doppler Current Profiler (ADCP) in the study of the circulation of the Adriatic Sea, *Ann. Geophys.*, *19*, 1183–1193.

Ursella, L., P.-M. Poulain, and R.P. Signell (2006), Surface drifter derived circulation in the northern and middle Adriatic Sea: Response to wind regime and season, *J. Geophys. Res.*, *111*, C03S04, doi:10.1029/2005JC003177. [printed *112* (C3), 2007]

Weller, R. A. (1982), The relation of near-inertial motions observed in the mixed layer during the JASIN [1978] experiment to the local wind stress and to the quasi-geostrophic flow field, *J. Phys. Oceanogr.*, *12*, 1122–1136.

Wunsch, C. (2006), *Discrete Inverse and State Estimation Problems, With Geophysical Fluid Applications*, 371 pp., Cambridge Univ. Press, New York.

C. Chavanne and P. Flament, Department of Oceanography, School of Ocean and Earth Science and Technology, University of Hawaii, 1000 Pope Road, Honolulu, HI 96822, USA. (cedric@hawaii.edu; pflament@soest.hawaii.edu)

K.-W. Gurgel, Institute of Oceanography, University of Hamburg, Bundesstrasse 53, D-20146 Hamburg, Germany.

I. Janeković and M. Kuzmić, Center for Marine and Environmental Research, Rudjer Bošković Institute, Bijenička 54, 10002 Zagreb, Croatia.

P.-M. Poulain, Istituto Nazionale di Oceanografia e di Geofisica Sperimentale, I-34010 Trieste, Italy.